

Finite-size effects in the diffusion dynamics of a glassforming binary mixture with large size ratio

Vinay Vaibhav,¹ Jürgen Horbach,² and Pinaki Chaudhuri¹

¹*The Institute of Mathematical Sciences, IV Cross Road,
CIT Campus, Taramani, Chennai 600 113, Tamil Nadu, India*

²*Institut für Theoretische Physik II: Weiche Materie,
Heinrich-Heine-Universität Düsseldorf, Universitätsstraße 1, 40225 Düsseldorf, Germany*

Extensive molecular dynamics (MD) computer simulations of an equimolar glassforming AB mixture with large size ratio are presented. While the large A particles show a glass transition around the critical density of mode coupling theory ρ_c , the small B particles remain mobile with a relatively weak decrease of their self-diffusion coefficient D_B with increasing density. Surprisingly, around ρ_c , the self-diffusion coefficient of the A particles, D_A , also starts to follow a rather weak dependence on density. We show that this is due to finite-size effects that can be understood from the analysis of the collective interdiffusion dynamics.

I. INTRODUCTION

Many soft matter systems as well as many biological systems consist of particles of very different sizes [1–3]. These systems may show a glassy dynamics with a time-scale separation of relaxation processes among the different constituents. Examples of such systems are glass-forming mixtures of small and large particles that have been studied experimentally via various colloidal and organic systems [4–10] and numerically via hard or soft sphere systems in computer simulations [11–15] as well as in the framework of mode-coupling theory (MCT) [16–18]. A common feature in these studies is a freezing of the large particles into a glass state while the small particles remain mobile. Here, the dynamics of the small particles is typically associated with anomalous diffusion on long transient time scales, as reflected, e.g., by a sub-linear growth of the mean-squared displacement $\delta r^2(t)$ as a function of time t , i.e. $\delta r^2(t) \propto t^\alpha$ with $\alpha < 1$. In computer simulations as well as experiments of disparate-sized mixtures [6, 7, 12, 19, 20], one finds values for the exponent α that in general depend on the temperature, the total density of the system, the concentration of small mobile particles, and the interactions between the particle, especially those between the large and the small particles. Thus, the values of α are non-universal and there is typically the lack of a sharp critical point at which one observes an asymptotic subdiffusive behavior in the longtime limit with a universal value of the exponent α . This non-universal behavior can be due to the thermal motion of the particles or soft interactions between small and large particles.

In a binary mixture of small and large particles, there are the two corresponding selfdiffusion coefficients D_s and D_l , respectively, that characterize on one hand the glassy dynamics of the large particles (D_l) and on the other hand the transport of the mobile small particles (D_s). However, in addition to these single-particle transport coefficients, there is also a collective diffusion coefficient, namely the interdiffusion coefficient D_{AB} , that characterizes the mass transport in the binary mixture [21–23].

In good approximation, D_{AB} can be often expressed as a simple linear combination of the selfdiffusion coefficients,

$$D_{AB} = \Phi(x_l D_s + x_s D_l), \quad (1)$$

with x_l and x_s the concentration of the large and the small particles, respectively, and Φ the thermodynamic factor (see below). Equation (1) is often called the Darken equation [24] or the Hartley-Crank equation [25]. Computer simulations of glassforming metallic systems Al-Ni and Zr-Ni with different compositions [23, 26] have shown that Eq. (1) qualitatively reproduces the temperature dependence of the interdiffusion coefficient, especially at low temperatures.

The question of whether the interdiffusion coefficient can be expressed in terms of the selfdiffusion coefficients has been extensively discussed in the literature, especially in the context of (binary) polymer mixtures [22, 27–31]. In this context, Eq. (1) is often referred to as the result of a “fast mode theory” [22], because according to Eq. (1) for a disparate-sized binary mixture the interdiffusion coefficient would be essentially given by the self-diffusion coefficient, D_s , of the fast mobile species. In a “slow mode theory”, however, the opposite behavior is predicted. Here, the relation between the interdiffusion and the selfdiffusion coefficients is given by [30]

$$D_{AB} = \frac{\Phi}{\frac{x_l}{D_s} + \frac{x_s}{D_l}}, \quad (2)$$

This result can be obtained in the framework of a random phase approximation [22]. It implies that in a disparate-sized mixture D_{AB} is dominated by the selfdiffusion coefficient of the slow species, D_l . Note that in the framework of MCT one also finds that D_{AB} tends to “follow” the slow species such that it always vanishes in a glass state [32].

For our study, we consider an equimolar binary AB mixture of soft spheres for which the size ratio of the two species is ≈ 2.85 and, in addition, the strength of the interaction between AB pairs is weaker than that between AA and BB pairs. In an earlier molecular dynamics (MD) simulation study of this system [12], it has been

demonstrated that on the typical time scale accessible in the MD simulation the A species falls out-of-equilibrium around the MCT critical number density which is at $\rho_c = 2.23$, corresponding to a number density of A particles $\rho_c^A = 1.115$. While the A species is in a frozen-in state above ρ_c , the B species remains mobile and there is a relatively weak decrease of the corresponding selfdiffusion coefficient D_B with increasing density above ρ_c . We demonstrate that Eq. (1) very well describes the density dependence of the interdiffusion coefficients and thus at high density D_{AB} is proportional to D_B .

We show that the approximative proportionality $D_{AB} \propto D_B$ is associated with strong finite-size effects of the selfdiffusion coefficient of the slow large species, D_A . These finite-size effects are due to the relation of D_{AB} to the diffusion coefficient of the centre of mass of species α (with $\alpha = A, B$), $D_{cm}^{(\alpha)}$. Note that $D_{cm}^{(A)} = D_{cm}^{(B)}$ holds because the total system's centre of mass is fixed. As we shall see below, $D_{cm}^{(A)} \propto D_{AB}/N$, with N the total number of particles in the system. Thus, the self-diffusion coefficient of the A species, D_A , has a finite-size correction $\propto D_{AB}/N \propto D_B/N$ that may be the dominant contribution to D_A for $\rho^A \gtrsim \rho_c^A$ and small system sizes. Only if one corrects the selfdiffusion coefficient D_A by computing it relative to the center of mass of the A species, one can extract the true value of D_A without the $1/N$ correction. As we argue below, similar features could be observed in any glassforming system with strong dynamic heterogeneities. In such systems, there can be clusters of slow particles with a relatively fast center-of-mass motion on time scales where no particle rearrangements inside the cluster occur. Therefore, our study reveals a common feature in the dynamics of glassforming liquids.

The rest of the paper is organized as follows: In Sec. II, we present the model of the AB mixture, the details of the simulation and quantities used to analyze the structure and dynamics of the system. The results of the analysis of structure and dynamics are given in Sec. III, followed by a summary and conclusions in Sec. IV.

II. MODEL AND METHODS

A. Interaction potential and details of the simulation

The system that we study [12] is a binary 50 – 50 mixture of repulsive particles, where the diameter of the bigger particles (species A) is sampled from a uniform distribution, i.e. $d_A \in [0.85, 1.15]$, while the diameter of the smaller particles (species B) is $d_B = 0.35$ (see Fig. 1). The average size ratio of A and B particles is $\langle d_A \rangle / d_B \approx 2.85$ where $\langle d_A \rangle \approx 1$. A pair of particles $\{\alpha, \beta\}$ (with $\alpha = A, B$ and $\beta = A, B$), separated by a distance r , interacts via a Weeks-Chandler-Andersen (WCA) potential [33], i.e. a Lennard-Jones potential that is cut off at its minimum and shifted to zero. To further smoothen the WCA potential, we also add a term that

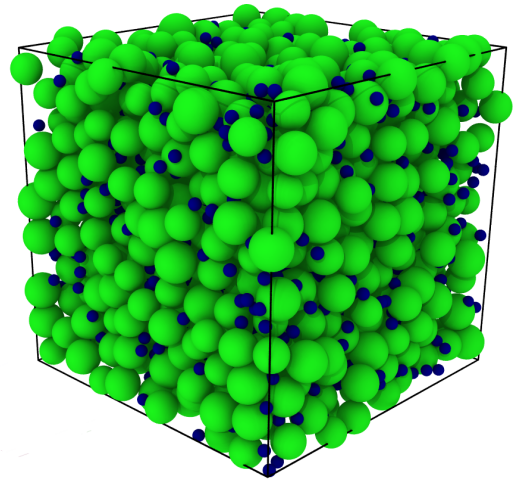


FIG. 1. Snapshot of the system at the density $\rho = 2.5$. A and B particles are represented by green and black spheres, respectively.

provides the continuity of its derivative. Thus, the potential is defined by

$$V_{\alpha\beta}(r) = u_{\alpha\beta}(r) - u_{\alpha\beta}(R_c) - (r - R_c) \left. \frac{du_{\alpha\beta}}{dr} \right|_{r=R_c},$$

$$u_{\alpha\beta}(r) = 4\epsilon_{\alpha\beta} \left[(\sigma_{\alpha\beta}/r)^{12} - (\sigma_{\alpha\beta}/r)^6 \right], \quad (3)$$

for $r < R_c = 2^{1/6}\sigma_{\alpha\beta}$, else $V_{\alpha\beta}(r) = 0$, with α, β as particle index. Here, $\sigma_{\alpha\beta} = (d_\alpha + d_\beta)/2$ and $\epsilon_{\alpha\beta} = \epsilon = 1.0$ if both interacting particles are of the same type, else $\sigma_{\alpha\beta} = (1.00 + 0.35)/2$ and $\epsilon_{\alpha\beta} = 0.1$. All particles have the same mass $m_A = m_B = m = 1$. In the following, length, energy, and time are measured in units of $\langle d_A \rangle$, ϵ , and $\tau_{WCA} = [m\langle d_A \rangle^2/\epsilon]^{1/2}$, respectively.

Using LAMMPS [34], extensive molecular dynamics (MD) simulations are performed for systems with $N = 1000, 2000$, and 4000 particles, placed in a three-dimensional cubic box with periodic boundary conditions. The equations of motion are integrated using the velocity form of the Verlet algorithm [35] with a time step $dt = 0.00075 \tau_{WCA}$. The simulations are done for different number densities in the range $2.1 \leq \rho \leq 3.5$ at the temperature $T = 2/3$. For each density, 30 independent samples are simulated. During the equilibration of the samples, the temperature is kept constant using a dissipative particle dynamics (DPD) thermostat [36] where the damping coefficient is set to 1.0. For the high densities, $\rho \geq 2.25$, the MD simulations are combined with the swap Monte Carlo (SMC) algorithm [37, 38] to obtain well-annealed samples. In a trial SMC move, one randomly selects a pair of particles, exchanges their diameters, and accepts or rejects this move according to a Metropolis criterion. In our scheme, only the diameters of the A particles are swapped. Every 100 MD steps, N_A trial SMC moves are done. The longest equilibration runs with the hybrid MD-SMC method were over

6×10^8 time steps. After the equilibration, the thermostat as well as the SMC are switched off, performing the production runs in the microcanonical ensemble.

A snapshot of the system at the density $\rho = 2.5$ is shown in Fig. 1. From this snapshot, one can infer that the large A particles form a close-packed structure while the small B particles can explore the free volume between the A particles.

B. Structural and dynamic properties

In this section, we define the correlation functions and transport coefficients that we use to analyse the simulation results for our AB mixture. A central static correlation function for our analysis is the concentration-concentration structure factor $S_{cc}(q)$. In the limit $q \rightarrow 0$, this function is related to the thermodynamic factor Φ in Eq. (1). After having introduced $S_{cc}(q)$ and its relation to Φ , we show how the selfdiffusion as well as the interdiffusion coefficients can be computed via Einstein relations, i.e. via long-time limits of mean-squared displacements.

We consider an AB mixture that contains a total number of $N = N_A + N_B$ particles. Thus, the concentration of A and B particles is given by $x_A = N_A/N$ and $x_B = N_B/N$, respectively. The local number density in reciprocal space for particles of type α can be defined as follows [39]:

$$\rho_\alpha(\vec{q}) = \sum_{j=1}^{N_\alpha} \exp(i\vec{q} \cdot \vec{r}_j) \quad (4)$$

with \vec{q} the wavevector and \vec{r}_j the position of the j 'th particle of type α . The autocorrelation functions of the density variables, as defined by Eq. (4), are the partial structure factors [39],

$$\begin{aligned} S_{\alpha\beta}(q) &= \frac{1}{N} \langle \rho_\alpha(\vec{q}) \rho_\beta(-\vec{q}) \rangle \\ &= \frac{1}{N} \sum_{j=1}^{N_\alpha} \sum_{k=1}^{N_\beta} \langle \exp[-i\vec{q} \cdot (\vec{r}_j - \vec{r}_k)] \rangle, \end{aligned} \quad (5)$$

where $\langle \cdot \rangle$ indicates an ensemble average. Note that we assume in Eq. (5) that the system is isotropic and thus the partial structure factors only depend on the magnitude of the wavevector, q .

From the densities (4), we can introduce local concentration fluctuation variables [39] as

$$c_\alpha(\vec{q}) = \rho_\alpha(\vec{q}) - x_\alpha (\rho_A(\vec{q}) + \rho_B(\vec{q})), \quad (6)$$

describing the local deviation from a homogeneous distribution of particles of type α . Since $c_A + c_B = 0$, the concentration variables are not independent of each other and it suffices to define *one* concentration-concentration structure factor for the binary mixture as

$$S_{cc}(q) = \frac{1}{N} \langle c_A(\vec{q}) c_A(-\vec{q}) \rangle. \quad (7)$$

This function can be also expressed as a linear combination of the partial structure factors,

$$S_{cc}(q) = x_B^2 S_{AA}(q) + x_A^2 S_{BB}(q) - 2x_A x_B S_{AB}(q). \quad (8)$$

In the limit $q \rightarrow \infty$, $S_{cc}(q)$ approaches $x_A x_B$, corresponding to the concentration-concentration structure factor of an ideal binary mixture. In the limit $q \rightarrow 0$, $S_{cc}(q)$ is related to the concentration susceptibility and thus to the second derivative of the Gibbs free energy G with respect to x_A and x_B via

$$\Phi = \frac{x_A x_B}{k_B T} \frac{\partial^2 G}{\partial x_A \partial x_B} = \frac{x_A x_B}{S(q=0)}, \quad (9)$$

with k_B the Boltzmann constant. Below, we use Eq. (9) to compute the thermodynamic factor from an extrapolation of $S_{cc}(q)$ to $q = 0$.

Now we introduce quantities that characterize dynamic properties of the AB mixture. At a single-particle level, we consider the incoherent intermediate scattering function $F_s^\alpha(q, t)$ of a tagged particle of type α . This is the correlation function of the time-displaced one-particle density and defined by [39]

$$F_s^\alpha(q, t) = \frac{1}{N_\alpha} \sum_{j=1}^{N_\alpha} \langle \exp[-i\vec{q} \cdot (\vec{r}_j(t) - \vec{r}_j(0))] \rangle. \quad (10)$$

Of special interest for the analysis of the dynamics of glassforming liquids is the decay of $F_s^\alpha(q, t)$ as a function of time around values of q corresponding to the location of the first peak of the static structure factor, q_{\max} . This is due to the fact that slowing down of the structural relaxation of the glassforming liquid is associated with the cage effect [40] and the typical size of a cage is of the order of $2\pi/q_{\max}$. In our case, the A particles exhibit a typical glassy dynamics and the first peak of $S_{AA}(q)$ is at $q_{\max} \approx 6$. Thus, below we consider $F_s^\alpha(q, t)$ at this value of q .

We determine the selfdiffusion coefficient of a tagged particle of type α from the mean-squared displacement (MSD), defined by

$$\langle \delta r_\alpha^2(t) \rangle = \frac{1}{N_\alpha} \sum_{j=1}^{N_\alpha} \langle (\vec{r}_j(t) - \vec{r}_j(0))^2 \rangle, \quad (11)$$

The corresponding selfdiffusion coefficient D_α is obtained from the long-time limit of $\langle \delta r_\alpha^2(t) \rangle$ via the Einstein relation [39, 40]

$$D_\alpha = \lim_{t \rightarrow \infty} \frac{\langle \delta \vec{r}_\alpha^2(t) \rangle}{6t}. \quad (12)$$

We also compute modified versions of the incoherent intermediate scattering function and the MSD where we replace the coordinates of the particles $\vec{r}_j(t)$ in Eqs. (10) and (11) by

$$\vec{r}_j'(t) = \vec{r}_j(t) - \vec{R}_A(t). \quad (13)$$

In this equation, $\vec{R}_A(t)$ is the center-of-mass coordinate of the A particles at time t ,

$$\vec{R}_A(t) = \frac{1}{N_A} \sum_{j=1}^{N_A} \vec{r}_j(t), \quad (14)$$

with \vec{r}_j the position of the j 'th particle of type A. The purpose of calculating $F_s^\alpha(q, t)$ and $\langle \delta r_\alpha^2(t) \rangle$ with the center-of-mass-corrected coordinates (13) will become clear below.

The interdiffusion coefficient D_{AB} can be also calculated from an Einstein relation, i.e. from the long-time limit of a MSD. In this case, the MSD of the variable $\vec{R}_A(t)$ has to be considered,

$$\langle \delta R^2(t) \rangle_{\text{cm}} = \left\langle \left[\vec{R}_A(t) - \vec{R}_A(0) \right]^2 \right\rangle. \quad (15)$$

Then, the interdiffusion coefficient is given by [23]

$$D_{AB} = \Phi L, \quad (16)$$

where Φ is the thermodynamic factor, as defined by Eq. (9), and the Onsager coefficient

$$L = \left[1 + \frac{x_A}{x_B} \right]^2 N x_A x_B \lim_{t \rightarrow \infty} \frac{\langle \delta R^2(t) \rangle_{\text{cm}}}{6t}, \quad (17)$$

describes the kinetic part of D_{AB} .

One can also define a center-of-mass diffusion coefficient for each species which, for species A, is given by

$$D_A^{\text{cm}} = \lim_{t \rightarrow \infty} \frac{\langle \delta R^2(t) \rangle_{\text{cm}}}{6t}. \quad (18)$$

For the mixture that is being studied, where $x_A = x_B = 1/2$, we therefore obtain $D_{AB} = \Phi N D_A^{\text{cm}}$ and $L = N D_A^{\text{cm}}$.

Formally, the interdiffusion coefficient D_{AB} can be written as a linear combination of the selfdiffusion coefficients,

$$D_{AB} = \Phi S (x_A D_B + x_B D_A), \quad (19)$$

where the ‘‘Manning factor’’ [41] S contains all the cross correlations [23] that contribute to L . The value $S = 1$ implies vanishing cross correlations [22, 23]. In this case, the Darken equation (1) holds.

III. RESULTS

A. Structural and thermodynamic properties

With the aid of the SMC technique, we are able to obtain well-annealed samples at very high densities that are above the critical MCT density $\rho_c \approx 2.23$ [12]. However, at such high densities, one may expect that at least for the A particles, the thermodynamic equilibrium is an

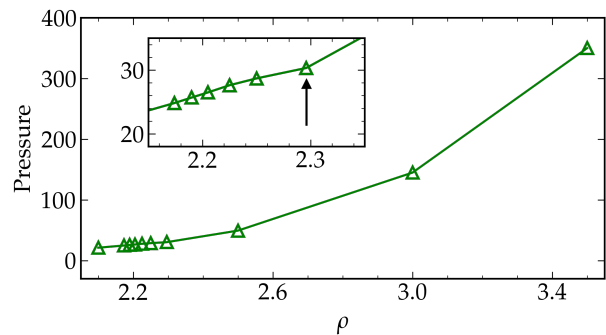


FIG. 2. Pressure P as a function of density. The inset zooms in the region around $\rho = 2.296$ (this density is indicated by an arrow).

ordered crystalline phase. Although the large polydispersity of the A particles in our model suppresses crystallization to some extent, the use of the SMC technique tends to also accelerate the formation of crystalline clusters and therefore we check especially the high-density samples whether they are purely amorphous structures and thus free of any crystalline clusters. To this end, we measure static structure factors and analyse the samples in terms of local bond order parameters. Furthermore, we determine the thermodynamic factor Φ from the concentration-concentration structure factor $S_{cc}(q)$.

The pressure P increases monotonously with increasing density ρ (Fig. 2). However, the lines connecting the points between $\rho = 2.25$ and $\rho = 2.296$ in $P(\rho)$ indicate a slight change of the slope (cf. the inset of Fig. 2). This could be due to a liquid-solid coexistence, occurring around these densities. And indeed our analysis for the density $\rho = 2.296$ (see below) indicates the occurrence of crystalline clusters in some of the samples at that density.

To quantify the structural changes in our AB mixture with increasing density, we now consider the partial structure factors $S_{\alpha\beta}(q)$. The top panels of Fig. 3 show these functions for different values of ρ . With increasing ρ , the first peak in both $S_{AA}(q)$ and $S_{BB}(q)$ shifts to larger q as the inter-particle separation decreases. In between, at the density $\rho = 2.296$, $S_{AA}(q)$ shows signatures of possible formation of local crystallites, with discrete spikes being clearly visible. Although less prominent, this is also reflected in the cross correlation, $S_{AB}(q)$, as well as in the total structure factor $S_{nn}(q) = S_{AA}(q) + S_{BB}(q) + 2S_{AB}(q)$ that is shown in the inset of the plot of $S_{AA}(q)$. However, for densities higher than $\rho = 2.296$ there is no sign of any Bragg peaks, suggesting that the samples at these high densities is purely amorphous. In fact, this is confirmed by our analysis of the samples in terms of local bond order parameters (see below).

In the bottom panel of Fig. 3, we show how $S_{cc}(q)$ varies with increasing density. We extract $S_{cc}(0)$ by extrapolating $S_{cc}(q)$ to $q = 0$, using the fit function $f(q) = S_{cc}(0)[1 - Aq^2 + Bq^4]$ (with $S_{cc}(0)$, A , and B

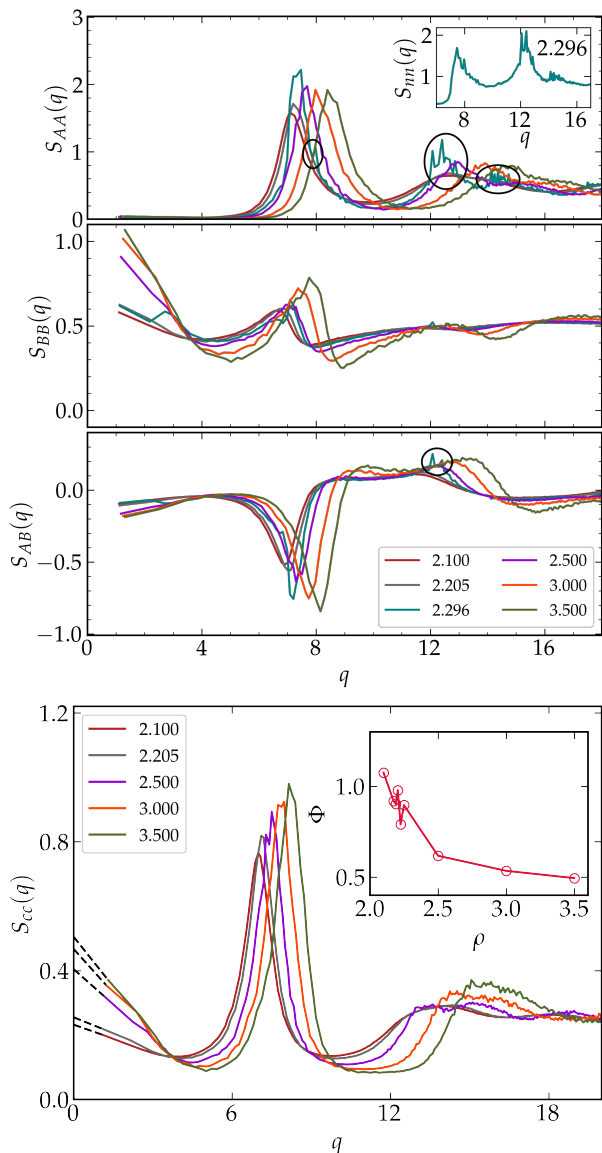


FIG. 3. **Top panels:** Partial structure factors $S_{AA}(q)$, $S_{BB}(q)$, and $S_{AB}(q)$ at different densities. Emerging Bragg peaks are indicated by circles. The inset of the plot of $S_{AA}(q)$ shows the total structure factor $S_{nn}(q)$ at the density $\rho = 2.296$. **Bottom panel:** Concentration-concentration structure factor $S_{cc}(q)$ at different densities. The dashed lines indicate the extrapolation to $q = 0$ via a fit function (see text). The thermodynamic factor Φ , as obtained from the fitted $S(q = 0)$, is shown in the inset as a function of density.

being fit parameters). For the fits (dashed lines), we have only taken into account the data for $q \leq 2.0$. Then, from $S_{cc}(0)$ we compute the thermodynamic factor Φ via Eq. (9). The variation of Φ is shown in the inset. We observe that Φ decreases from a value of about 1.0 at $\rho = 2.0$ to a value of about 0.5 at the highest considered density, $\rho = 3.5$. This rather weak variation of Φ over a broad range of densities also implies that the thermody-

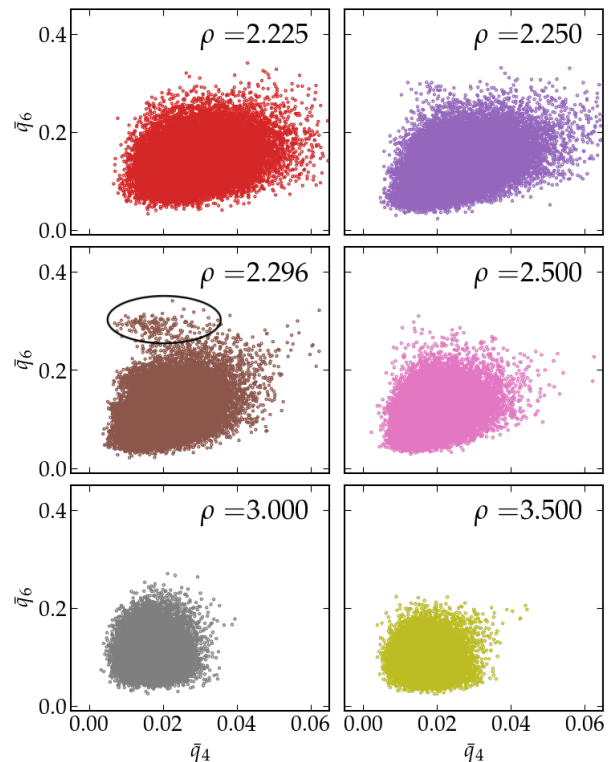


FIG. 4. $\bar{q}_4 - \bar{q}_6$ plot for system at different marked densities (calculation with cutoff). The closed line in the plot for $\rho = 2.296$ indicates the values of $\bar{q}_4 - \bar{q}_6$ pairs that correspond to crystalline BCC clusters (see text).

amic factor does not strongly affect the density dependence of the interdiffusion coefficient, which we discuss further below.

Our analysis to check for local crystalline order is based on the local bond order parameters that have been proposed by Steinhardt *et al.* [42]. For such analysis, at first we identify the nearest neighbours for each particle within the cutoff 1.5 ($N_b(i)$ is the number of such neighbours for each particle i). After this, for each particle, a complex local orientational order vector $q_{lm}(i)$ with $(2l + 1)$ components is constructed using the following definition:

$$q_{lm}(i) = \frac{1}{N_b(i)} \sum_{j=1}^{N_b(i)} Y_{lm}(\vec{r}_{ij}). \quad (20)$$

Here, $Y_{lm}(\vec{r}_{ij})$ is the spherical harmonic of degree l and order m . As per definition, l is always a non-negative integer and m can take the integral values from $m = -l$ to $m = l$ for a given value of l . Also, \vec{r}_{ij} is the vector from the particle i to particle j . Now, as suggested in Ref. [43], the locally averaged quantity $\bar{q}_{lm}(i)$ is calculated for each particle i , using

$$\bar{q}_{lm}(i) = \frac{1}{\tilde{N}_b(i)} \sum_{k=0}^{\tilde{N}_b(i)} q_{lm}(k), \quad (21)$$

where averaging (summation from $k = 0$ to $\tilde{N}_b(i)$) has been done over the neighboring particles of i (as above defined, based on the cutoff) and particle i itself. Such averaging procedure takes into account even the information of the structure beyond the cutoff and has shown better identification of crystal structures in simulations. Using these averaged form of local bond order vector components a norm $\bar{q}_l(i)$ is defined for each particle:

$$\bar{q}_l(i) = \sqrt{\frac{4\pi}{2l+1} \sum_{m=-l}^l |\bar{q}_{lm}(i)|^2}. \quad (22)$$

Depending on the definition of the spherical harmonics used, the factor $\frac{4\pi}{2l+1}$ before summation in the above equation, is used or not used. This quantity $\bar{q}_l(i)$ is sensitive to different crystal structure systems depending on the choice of l . Specially, bond orientational order parameter for $l = 4$ and $l = 6$ have been used to identify structures similar to cubic and hexagonal systems. We have calculated the correlation between \bar{q}_4 and \bar{q}_6 for the A particles in our system.

The measured values of \bar{q}_4 and \bar{q}_6 , for each particle across several representative configurations, can be visualized in the form of a scatter plot in the \bar{q}_4 - \bar{q}_6 plane, following Ref. [43], to check if local environments exhibit any formation of ordered structures. This is shown in Fig. 4, for a few densities across the range that we have studied, using configurations sampled from 30 independent trajectories. First thing to notice is that, across all the densities, the values of \bar{q}_4 are small (< 0.06) and in fact shrink with increasing density. Similarly for \bar{q}_6 , the numbers are in the liquid-like regime, except for $\rho = 2.296$ where some pockets of BCC-like structures seem to be visible for some clusters within some trajectories, if we compare with observations reported in Ref. [43].

To summarize, the structural changes with increasing density are on expected lines. There is some hint of occurrence of a small number of local crystallites, in the vicinity of the mode coupling density. However, when supercooled to higher densities, the system remains disordered, even when equilibrated via SMC.

B. Diffusion dynamics

We will now discuss the dynamic properties of the mixture. As mentioned earlier, for the model system that we are studying, the larger A species are known to exhibit a mode coupling transition around $\rho_c \approx 2.23$ [12]. For $\rho \gtrsim \rho_c$, the A particles are essentially in a frozen-in configuration on the diffusive time scale of the B particles. However, the diffusivity of the B particles also continues to decrease with increasing density such that they are expected to be in an arrested state at very large densities.

In the following, our main objective is to study the density dependence of the interdiffusion coefficient. To

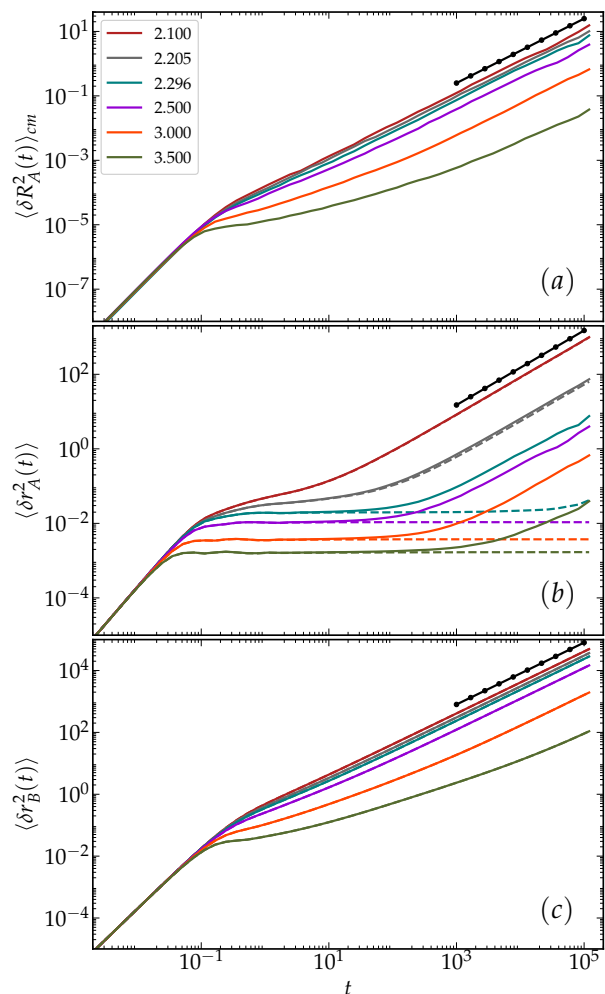


FIG. 5. (a) Center-of-mass MSD, $\langle \delta R^2(t) \rangle_{cm}$, for different densities. (b) Single-particle MSDs of A species and (c) of B species for the same densities. In b) and c), solid and dotted lines represent calculations with and without the center-of-mass correction, respectively (see text). In all sub-plots, the solid lines with dots are straight lines $\propto t$ to indicate the diffusional regime of the MSDs at long times.

this end, one has to monitor the trajectory of the center of mass of the A species and the corresponding time evolution of $\langle \delta R^2(t) \rangle_{cm}$, as defined by Eq. (15), needs to be computed. This MSD is shown in Fig. 5a for different densities. For the same densities, Figs. 5b and 5c display the single-particle MSDs, $\langle \delta r_\alpha^2(t) \rangle$ (see Eq. (11)), of the A and B particles, respectively. For the A species, $\langle \delta r_A^2(t) \rangle$ shows the behaviour that is expected for a typical glassforming liquid. There is a short-time ballistic regime ($\propto t^2$) and a long-time diffusive regime ($\propto t$). In between these two regimes, there is a plateau-like region that becomes more pronounced and broader with increasing density. The latter regime is due to the intermediate caging of the particles. Importantly, we note that even for $\rho > \rho_c$, the MSD of A particles still displays diffusive dynamics at long times. Below, we show that this feature

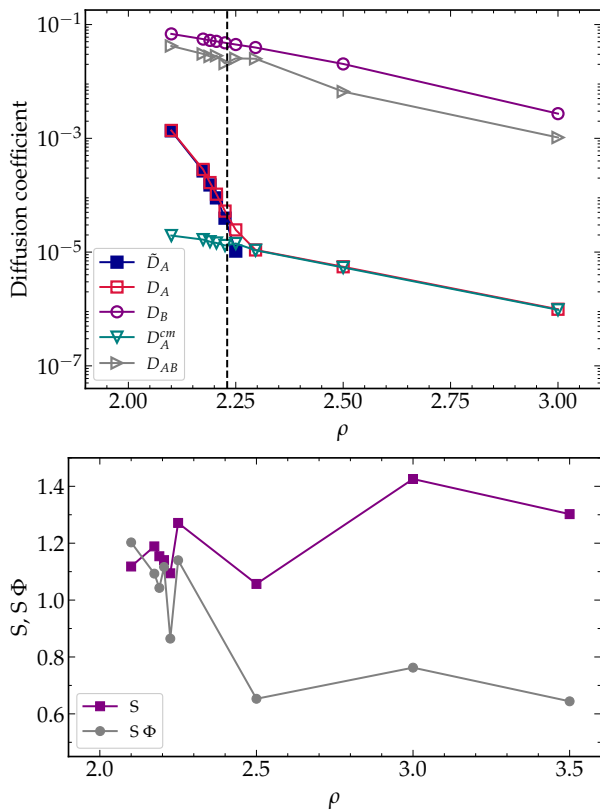


FIG. 6. **Top panel:** Selfdiffusion coefficients D_A and D_B , the center-of-mass diffusion coefficient D_A^{cm} and the interdiffusion coefficient D_{AB} as a function of density ρ . Also shown is the rectified self-diffusion coefficient \tilde{D}_A (see text). The vertical dashed line marks the previously estimated critical MCT density for D_A at $\rho_c = 2.23$. **Bottom panel:** Manning factor S and the product $S\Phi$ as a function of density.

is a finite-size effect, i.e. the observed diffusive regime for $\rho > \rho_c$ shifts to longer time scales with increasing system size. For the case of B species, the shape of the MSD, i.e. of $\langle \delta r_B^2(t) \rangle$, is very different from that of the A particles, with no intermediate plateau at all. We will also discuss this, below. Now, if we look at the MSD curves for the center-of-mass motion, it is evident that they bear close resemblance with that of the B species, the reason for which will be evident once we analyse the diffusion coefficients.

The long-time dynamical behaviour is well characterized by measuring the respective diffusion coefficients, measured from the corresponding MSD data, as defined in Eqs. (12), (16), and (18). The density variation of the measured single-particle diffusion coefficients, D_A and D_B , the center-of-mass diffusion coefficient D_A^{cm} as well as the interdiffusion coefficient D_{AB} are shown in Fig. 6. First, we note that the diffusion coefficient of the smaller B particles remains finite beyond ρ_c (indicated via the dashed vertical line), consistent with previous study [12]. Now, if we look at the data for D_A , we observe that it decreases as it approaches ρ_c , as reported earlier, and be-

yond that there seems to be a separate branch of weaker decrease with density. Interestingly, for $\rho > \rho_c$, the measured center-of-mass diffusion coefficient, D_A^{cm} , shows exactly the same density dependence. As already noted in the previous paragraph, the measured interdiffusion coefficient has a density dependence which resembles that of the diffusivity of B species, over the entire density range.

We now analyse the motion of A particles for $\rho > \rho_c$. Since the density dependence of D_A , in this density regime, matches that of D_A^{cm} , it implies that the observed motion of the individual A particles is actually due to the motion of the center of mass of the A species. To disentangle that, we compute the MSD of the A particles by shifting to the frame of reference of the population's center of mass, see Eq. (13). The redefined MSDs are plotted in the top panel of Fig. 5, using dashed lines. We observe that following this rectification, there is a significant change in the MSD for $\rho > \rho_c$. The rectified MSDs, in that regime, exhibit a prolonged plateau over the time window of our observation implying that in the frame of reference of the center of mass, the particles are essentially caged and there is hardly any cage-breaking, especially for $\rho \geq 2.5$. Therefore, we can conclude that only due to the motion of the center of mass, deviations from the plateau are exhibited in the bare MSDs at these densities. At small enough density ($\rho = 2.1$), this rectification is not observed, and there is a mild rectification for $\rho = 2.205$. The rectified selfdiffusion coefficient of the A particles is also shown in Fig. 6, from which it is evident that the rectified D_A , labelled as \tilde{D}_A , sharply decreases around ρ_c .

Having clarified the actual density dependence of D_A , we can now use Eq. (19) to analyse the behaviour of the interdiffusion coefficient. If the Manning factor is $S = 1.0$, Eq. (19) reduces to the Darken equation (1). Then, when $D_A = 0$, $D_{AB} \sim D_B$, which explains the observed behaviour of the interdiffusion coefficient in the regime $\rho \gg \rho_c$. Physically, even though there is a dynamical arrest of the A species, because of momentum conservation, the mobility of B species leads to the center-of-mass motion of the A species and the consequent finite interdiffusion coefficient. We also note that even at lower densities, $D_B > D_A$, and thus there too, the behaviour of D_{AB} is also dependent on the diffusive motion of the smaller but faster B particles.

Furthermore, we test the validity of the Darken approximation for the mixture that we are studying. To do that, we consider two different quantities, viz $S = D_{AB}/(x_A D_B + x_B D_A)$ and $S\Phi$, which are plotted in the bottom panel of Fig. 5. If the Darken approximation works, then S should be around 1. As we can infer from Fig. 5, over the whole range of densities, both S and $S\Phi$ deviate from unity by less than a factor of 2, while the interdiffusion coefficient decreases by about two orders of magnitude. So neither the cross correlations nor the thermodynamic factor strongly affect the density dependence of D_{AB} which is therefore essentially given by the linear combination of selfdiffusion coeffi-

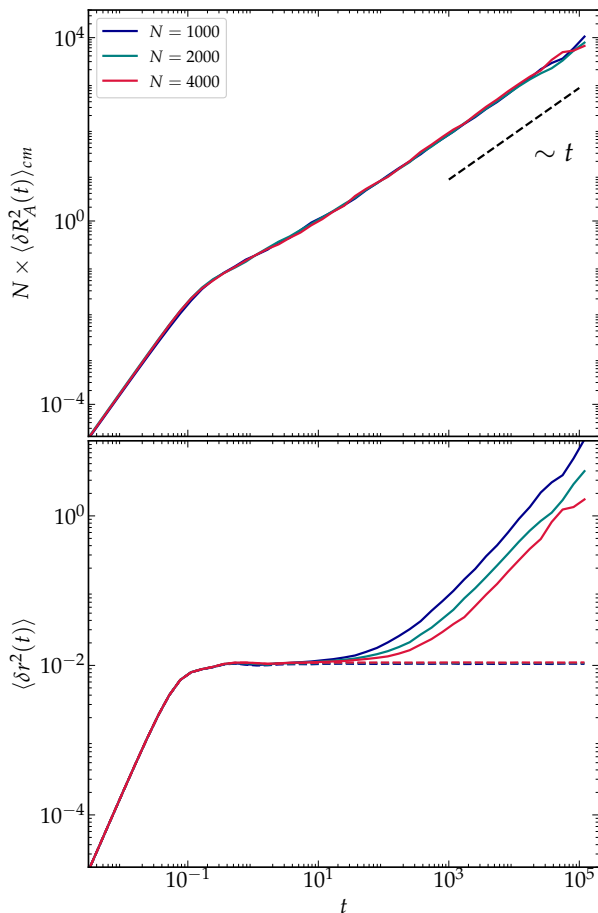


FIG. 7. **Top panel:** Center-of-mass MSD for A species, scaled with system size N , at density $\rho = 2.5$. **Bottom panel:** Single particle MSD of the A species at the same density, for the different system sizes. Solid and dotted lines represent calculations without and with center-of-mass correction, respectively.

cients, i.e. $D_{AB} \approx 0.5(D_A + D_B)$.

In the above discussions, we have noted that the MSD curves for B species do not show any plateau-like feature, i.e. the absence of any signatures of caging by neighbouring particles. Rather, these curves show anomalous intermediate sub-diffusive dynamics prior to diffusion. This is similar to what is observed in the case of interacting particles moving in a quenched environment of soft obstacles [19, 44]. For the binary mixture that we are studying, this is a reasonable scenario considering the large size ratio (see Fig. 1 for the visualisation). At the large density beyond ρ_c where we are probing the dynamics, the A population is nearly frozen, and the B particles are diffusing through this quenched environment with which they interact via some soft interaction. For the case of interacting particles moving in a quenched environment of soft obstacles, an avoided localization transition is observed [19], and one would expect a similar situation for the eventual dynamical arrest of the B species at large

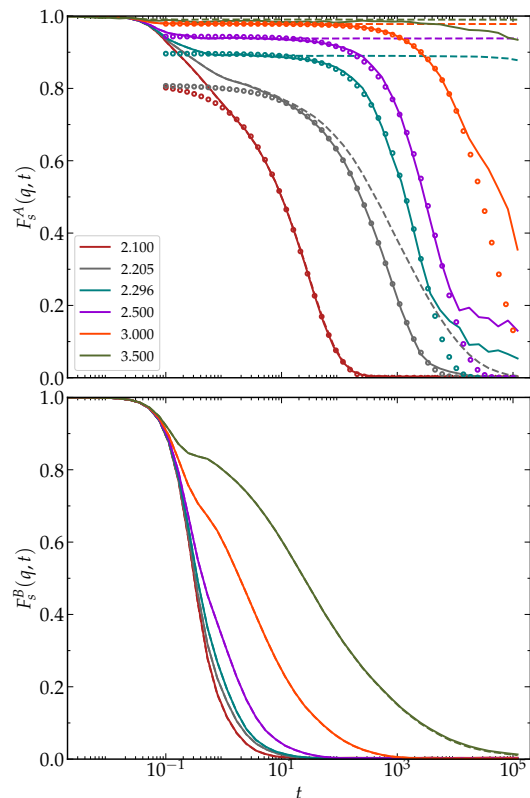


FIG. 8. Self-intermediate scattering function, $F_s^\alpha(q, t)$, for bigger A (top) and smaller B (bottom) particles, measured at $q = 6$, for different densities. In the top panel, solid and dashed lines represent calculations without and with center-of-mass correction, respectively. The dotted lines are fits with stretched exponentials (see text). The values of the stretching exponent are $\beta = 0.73, 0.68, 0.89, 0.86,$ and 0.87 for the densities $\rho = 2.1, 2.205, 2.296, 2.5,$ and 3.0 , respectively.

enough densities [12].

Next, we analyse the finite size effects in the measured diffusivities. Since the interdiffusion coefficient can be written as $D_{AB} = \Phi L$, where $L = ND_A^{cm}$, as discussed in the previous section, D_{AB} has no finite size effects. This is illustrated in the top panel of Fig. 7, where we plot the center-of-mass MSD of A species scaled with system size, at density of $\rho = 2.5$, for a density larger than ρ_c . We observe that the curves for the different system sizes collapse for the scaled MSD, implying that ND_A^{cm} is the same and therefore D_{AB} remains unaffected. On the other hand, the bare single particle MSDs show system size dependence at the same density, as shown in the bottom panel of Fig. 7. However, if we now measure the MSD of the particles in the frame of reference of the center of mass of the A particles, see Eq. (13), we observe that all collapse on the same plateau; see top panel of Fig. 7. This implies, that the finite size dependence in the single particle dynamics is coming from the change in centre-of-mass motion. However, as discussed above, this effect gets scaled out when computing the interdiffusion

coefficient.

So far, we have been discussing the anomalous effects in the mean squared displacement for $\rho > \rho_c$ and the rectification that is needed. This is also the case in other dynamical observables. In the top panel of Fig. 8, we illustrate this for the incoherent intermediate scattering function $F_s^A(q, t)$ at a wavenumber of $q = 6$, corresponding to correlations on nearest-neighbour distances. The bare measurements are shown with solid lines and the rectified curves as dashed lines, i.e. measurements done in the frame of reference of the center of mass. Consistent with the MSD data, at low densities (here $\rho = 2.1$), the bare and the rectified $F_s^A(q, t)$ coincide, while at higher densities the rectified function shows a slower and a more stretched decay (cf. the curves for $\rho = 2.205$). For $\rho \geq \rho_c$, the center-of-mass-corrected functions show extended plateaus in time, reflecting that in the frame of reference of the center of mass, the A particles are stuck in their locations.

The bare curves show a relaxation process, which can be fitted with stretched exponential functions, $f(q, t) = A_{\text{sef}} \exp[-(t/\tau_q)^\beta]$ (with A_{sef} , τ_q , and β being fit parameters). The values of the exponent β , as obtained from the fits, are in the range between 0.7 and 0.9 (see caption of Fig. 8). With increasing density, the stretching exponent β tends to increase towards 1.0, i.e. towards a simple exponential decay. This decay of $F_s^A(q, t)$ at $q = 6.0$ reflects the center-of-mass motion of the A species. At very long times, however, there is the crossover to a much slower decay, which is due to the fact that there are no rearrangements in the configuration of A particles. The bottom panel of Fig. 8 shows $F_s^B(q, t)$. Here, for the low densities, the decay happens very quickly. Only for $\rho > \rho_c$, the relaxation timescales start increasing significantly.

IV. SUMMARY AND CONCLUSIONS

Our work elucidates several aspects of the diffusion dynamics in an equimolar glassforming binary soft-sphere mixture with large size ratio. We observe a very pronounced time scale separation between the motion of the slow A species and that of the fast B species at high densities. As a consequence, the A particles show the typical glassy dynamics of a densely packed system, while the B particles remain mobile at very high densities, $\rho > \rho_c$, exploring the void space in between the A particles. We have seen that the interdiffusion coefficient D_{AB} can be well approximated by the Darken equation (1). Since at high density $D_A \ll D_B$, one therefore obtains $D_{AB} \approx \Phi x_A D_B$, i.e. the interdiffusion coefficient is dominated by the fast species. For our equimolar mixture, we can also write $D_{AB} = \Phi N D_A^{\text{cm}}$ and thus at high density we have $D_A^{\text{cm}} \approx D_B/(2N)$. This implies that even if the A particles form a frozen-in structure with essentially no rearrangements of the relative positions of particles, they may follow collectively the diffusive motion of their center of mass and one finds for the selfdiffusion coefficient $D_A \approx D_A^{\text{cm}} \propto N^{-1}$. One can, of course, correct for this finite-size effect by computing one-particle quantities such as $\langle \delta r_A^2(t) \rangle$ and $F_s^A(q, t)$ from the center-of-mass-corrected coordinates, as defined by Eq. (13).

The finite-size effects, that we have reported in this work with respect to the selfdiffusion coefficient of the slow species, are expected to be a typical feature in glass-forming binary mixtures with large size ratio. Moreover, one may expect similar effects in any glassforming system with strong dynamic heterogeneities.

ACKNOWLEDGMENTS

We thank IMSc HPC facility for providing computational resources for our work.

-
- [1] C. Bechinger, F. Sciortino, and P. Zihlerl (eds.), *Physics of Complex Colloids* (IOS Press, Amsterdam, 2013).
 - [2] M. Weiss, in *New Models of the Cell Nucleus: Crowding, Entropic Forces, Phase Separation, and Fractals*, edited by R. Hancock and K. W. Jeon, International review of cell and molecular biology Vol. 307 (Academic Press, San Diego, CA, 2014), Chap. 11, pp. 383–417.
 - [3] F. Höfling and T. Franosch, *Rep. Prog. Phys.* **76**, 046602 (2013).
 - [4] A. Imhof and J. K. G. Dhont, *Phys. Rev. Lett.* **75**, 1662 (1995).
 - [5] A. Imhof and J. K. G. Dhont, *Phys. Rev. E* **52**, 6344 (1995).
 - [6] R. Kurita and E. R. Weeks, *Phys. Rev. E* **82**, 041402 (2010).
 - [7] T. Blochowicz, S. Schramm, S. Lusceac, M. Vogel, B. Stühn, P. Gutfreund, and B. Frick, *Phys. Rev. Lett.* **109**, 035702 (2012).
 - [8] S. P. Bierwirth, C. Gainaru, and R. Böhmer, *J. Chem. Phys.* **149**, 044509 (2018).
 - [9] T. Sentjabrskaja, E. Zaccarelli, C. De Michele, F. Sciortino, P. Tartaglia, T. Voigtmann, S. U. Egelhaaf, and M. Laurati, *Nat. Commun.* **7**, 11133 (2016).
 - [10] E. Martinez-Sotelo, M. A. Escobedo-Sánchez, and M. Laurati, *J. Chem. Phys.* **151**, 164504 (2019).
 - [11] A. J. Moreno and J. Colmenero, *J. Chem. Phys.* **125**, 164507 (2006).
 - [12] J. Horbach, and T. Voigtmann, *Phys. Rev. Lett.* **109**, 205901 (2009).
 - [13] W.-S. Xu, Z.-Y. Sun, and L.-J. An, *J. Chem. Phys.* **137**, 104509 (2012).
 - [14] W.-S. Xu, Z.-Y. Sun, and L.-J. An, *Soft Matter* **11**, 627 (2015).
 - [15] E. Lázaro-Lázaro, J. A. Perera-Burgos, P. Laermann, T.

- Sentjabrskaja, G. Pérez-Ángel, M. Laurati, S. U. Egelhaaf, M. Medina-Noyola, T. Voigtmann, R. Castaneda-Priego, and L. F. Elizondo-Aguilera, *Phys. Rev. E* **99**, 042603 (2019).
- [16] J. Bosse and J. S. Thakur, *Phys. Rev. Lett.* **59**, 998 (1987).
- [17] J. Bosse and Y. Kaneko, *Phys. Rev. Lett.* **74**, 4023 (1995).
- [18] T. Voigtmann, *Europhys. Lett.* **96**, 36006 (2011).
- [19] S. K. Schnyder and J. Horbach, *Phys. Rev. Lett.* **120**, 078001 (2018).
- [20] J. Kurzidim, D. Coslovich, and G. Kahl, *J. Phys.: Condens. Matter* **23**, 234122 (2011).
- [21] D. D. Fitts, *Non-equilibrium Thermodynamics* (MacGraw-Hill, New York, 1962).
- [22] A. Z. Akcasu, *Macromol. Theory Simul.* **6**, 679 (1997).
- [23] J. Horbach, S. K. Das, A. Griesche, M.-P. Macht, G. Frohberg, and A. Meyer, *Phys. Rev. B* **75**, 174304 (2007).
- [24] L. S. Darken, *Trans. AIME* **180**, 430 (1949).
- [25] G. S. Hartley and J. Crank, *Trans. Faraday Soc.* **45**, 801 (1949).
- [26] P. Kuhn, J. Horbach, F. Kargl, A. Meyer, and Th. Voigtmann, *Phys. Rev. B* **90**(2), 024309 (2014).
- [27] R. J. Bearman, *J. Chem. Phys.* **32**, 1308 (1960).
- [28] F. Brochard and P. G. de Gennes, *Europhys. Lett.* **1**, 221 (1986).
- [29] H. Sillescu, *Makromol. Chem., Rapid Commun.* **8**, 393 (1987).
- [30] W. Hess, G. Nägele, and A. Z. Akcasu, *J. Polym. Sci., Part B: Polym. Phys.* **28**, 2233 (1990).
- [31] A. Z. Akcasu, G. Nägele, and R. Klein, *Macromolecules* **24**, 4408 (1991).
- [32] A. Latz, *Verallgemeinerte konstituierende Gleichungen und Formfaktoren für einfache Glasbildner*, Ph.D. thesis, TU München, Germany, 1990.
- [33] J. D. Weeks, D. Chandler, and H. C. Andersen, *J. Chem. Phys.* **54**, 5237 (1971).
- [34] S. Plimpton, *J. Comp. Phys.* **117**, 1 (1995).
- [35] M. P. Allen and D. J. Tildesley, *Computer Simulation of Liquids, 2nd ed.* (Oxford University Press, Oxford, 2017).
- [36] T. Soddemann, B. Dünweg, and K. Kremer, *Phys. Rev. E* **68**, 046702 (2003).
- [37] T. S. Grigera and G. Parisi, *Phys. Rev. E* **63**, 045102 (2001).
- [38] L. Berthier, E. Flenner, C. J. Fullerton, C. Scalliet, and M. Singh, *J. Stat. Mech.* 064004 (2019).
- [39] J.-P. Hansen and I. R. McDonald, *Theory of Simple Liquids* (Academic Press, London, 1986).
- [40] K. Binder and W. Kob, *Glassy Materials and Disordered Solids: An Introduction to Their Statistical Mechanics, Rev. Ed.* (World Scientific, Singapore, 2011).
- [41] J. R. Manning, *Phys. Rev.* **124**, 470 (1961).
- [42] P. J. Steinhardt, D. R. Nelson, and M. Ronchetti, *Phys. Rev. B* **28** (2), 784 (1983).
- [43] W. Lechner and C. Dellago, *J. Chem. Phys.* **129**, 114707 (2008).
- [44] S. K. Schnyder, M. Spanner, F. Höfling, T. Franosch, and J. Horbach, *Soft Matter* **11**, 701 (2015).